

A Neural Receiver for 5G NR Multi-user MIMO

Sebastian Cammerer¹, Fayçal Aït Aoudia¹, Jakob Hoydis¹, Andreas Oeldemann², Andreas Roessler²,
Timo Mayer², and Alexander Keller¹

¹NVIDIA, ²Rohde & Schwarz, contact: scammerer@nvidia.com

Abstract—We introduce a neural network (NN)-based multi-user multiple-input multiple-output (MU-MIMO) receiver with 5G New Radio (5G NR) physical uplink shared channel (PUSCH) compatibility. The NN architecture is based on convolution layers to exploit the time and frequency correlation of the channel and a graph neural network (GNN) to handle multiple users. The proposed architecture adapts to an arbitrary number of sub-carriers and supports a varying number of multiple-input multiple-output (MIMO) layers and users without the need for any retraining. The receiver operates on an entire 5G NR slot, i.e., processes the entire received orthogonal frequency division multiplexing (OFDM) time-frequency resource grid by jointly performing channel estimation, equalization, and demapping. The proposed architecture operates less than 1 dB away from a baseline using linear minimum mean square error (LMMSE) channel estimation with K-best detection but benefits from a significantly lower computational complexity. We show the importance of a carefully designed training process such that the trained receiver is universal for a wide range of different unseen channel conditions. Finally, we demonstrate the results of a hardware-in-the-loop verification based on 3GPP compliant conformance test scenarios.

I. INTRODUCTION

Artificial intelligence (AI) and machine learning (ML) have become ubiquitous tools in the wireless research community [1], [2] as well as the telecommunications industry [3]. This trend has been further accelerated by the recent announcement of the 3rd Generation Partnership Project (3GPP) consortium to investigate AI/ML in the physical layer as new study item for the upcoming 3GPP release 18 [3]. While this will most likely require disruptive changes in the signal structures and the transmitter implementation, our approach takes a different direction and focuses on neural network (NN)-based receivers which are fully compliant with 5G New Radio (5G NR). We emphasize that neural receivers can be seen as enabling technology for various novel applications such as site-specific basestations that can be re-trained after deployment as well as pilotless communications [4].

The concept of such a neural receiver was first proposed in [1] where the authors have demonstrated a performance close to that of a *classical* receiver with perfect channel state information (CSI) in a single-input multiple-output (SIMO) system by enabling joint channel estimation and data reconstruction. Note that earlier, the authors of [5] proposed convolutional neural network (CNN)-based receiver algorithms for OFDM detection. The neural receiver idea was extended to multiple-input multiple-output (MIMO) systems in [6]. It was shown

later in [4], that a similar architecture also permits pilotless communications when combined with end-to-end learning [2]. Further, neural receivers for internet of things (IoT) applications have been demonstrated [7]. However, when considering deep learning for multi-user multiple-input multiple-output (MU-MIMO) systems [8]–[11], often perfect CSI has been assumed, neglecting the issue of implicit channel estimation. In addition, it is unclear whether evaluations performed on simplistic channel models generalize to more challenging channel environments.

In this work, we extend the concept of neural receivers by a flexible MU-MIMO component with 5G NR physical uplink shared channel (PUSCH) compatibility. A specific focus of the NN architecture is on the flexibility with respect to a varying number of users and a configurable number of sub-carriers. The NN architecture itself is a combination of graph neural network (GNN) and CNN layers. Intuitively, the GNN offers flexibility regarding varying number of users as it allows an easy reconfiguration similar to [10]. As a result, approximately 730k trainable weights are required to process an entire 5G NR slot, meaning the entire time/frequency resources consisting of thousands of resource elements in the time-frequency grid of an orthogonal frequency division multiplexing (OFDM) system. The number of physical resource blocks (PRBs) is also variable - in fact, our receiver is trained for 4 PRBs but evaluated for 217 PRBs. This flexibility is a key enabler for practical deployment as the proposed architecture neither requires any retraining if a different number of users is scheduled, nor if the number of allocated sub-carriers changes.

A practical challenge is to train the system such that it does not overfit to the underlying dataset or channel model. We therefore randomize the channel during training by using system level 3GPP urban microcell (UMi) channel models with random user drops to ensure that the learned receiver generalizes to unseen channel conditions. The neural receiver and our experiments are implemented using Sionna [12].

II. NEURAL MULTI-USER MIMO OFDM RECEIVER

We consider a MU-MIMO OFDM communication system in which N_T MIMO *layers*¹ are simultaneously transmitted on the same physical resources to a single receiver with N_{RX} receive antennas. We assume a total number of N_{TX} transmit antennas. Such a communication system is illustrated in Fig. 1.

This work has received financial support from the European Union under Grant Agreement 101096379 (CENTRIC). Views and opinions expressed are however those of the author(s) only and do not necessarily reflect those of the European Union or the European Commission (granting authority). Neither the European Union nor the granting authority can be held responsible for them.

¹In 5G NR, each user – possibly equipped with multiple antennas – can be configured to transmit multiple MIMO *layers* (or data *streams*). For readability, we denote every layer as an independent transmitter in the following description. The proposed neural receiver architecture supports multiple layers per user by treating every stream as a (virtual) user.

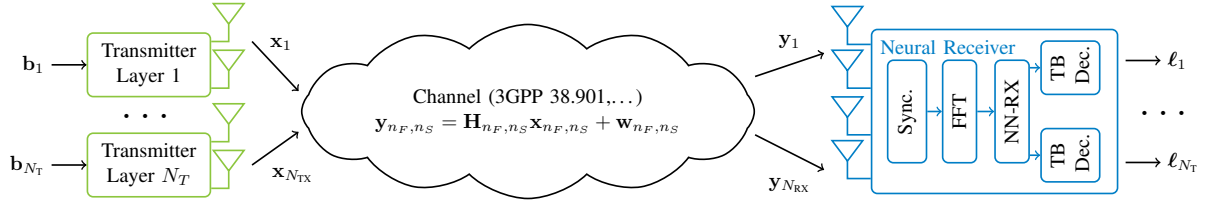


Fig. 1: Overview of an MU-MIMO OFDM communication system where N_T MIMO layers are received by N_{RX} antennas.

The problem of MU-MIMO detection is to reconstruct the bits transmitted by the individual layers from the received signal \mathbf{y} . We denote by N_S and by N_F the number of OFDM symbols and subcarriers forming the resource grid (RG), respectively. The n_T^{th} layer ($1 \leq n_T \leq N_T$) transmits a vector $\mathbf{b}_{n_F, n_S, n_T} \in \{0, 1\}^m$ of m bits on every resource element (RE) $[n_F, n_S]$ allocated to data transmission, where $1 \leq n_F \leq N_F$ and $1 \leq n_S \leq N_S$. To that aim, every vector $\mathbf{b}_{n_F, n_S, n_T}$ is mapped onto a complex-valued baseband symbol denoted by $\mathbf{x}_{n_F, n_S, n_T} \in \mathbb{C}$ which is typically done by using a 2^m quadrature amplitude modulation (QAM) with Gray labeling. MIMO precoding can be applied if a user has more than one transmit antenna. This leads to the OFDM RG of baseband modulated symbols

$$\mathbf{X}_{n_T} = \begin{bmatrix} \mathbf{x}_{1,1,n_T} & \cdots & \mathbf{x}_{1,N_S,n_T} \\ \vdots & \ddots & \vdots \\ \mathbf{x}_{N_F,1,n_T} & \cdots & \mathbf{x}_{N_F,N_S,n_T} \end{bmatrix}. \quad (1)$$

Some positions in \mathbf{X}_{n_T} are not used for data transmission but send known pilots, so-called demodulation reference signal (DMRS) pilots. We denote the set of pilot positions as \mathcal{P}_{n_T} for each layer n_T where each $\mathbf{p}_{n_T} \in \mathcal{P}_{n_T}$ is given as $\mathbf{p}_{n_T} = [p_F, p_S] \in \mathbb{N}^2$ defining the indices of pilot positions in the RG.

We assume OFDM with a sufficiently long cyclic prefix (CP) duration. Hence, the received RG is denoted by $\mathbf{Y} = \{\mathbf{y}_{n_F, n_S}\}_{1 \leq n_F \leq N_F, 1 \leq n_S \leq N_S}$, where $\mathbf{y}_{n_F, n_S} \in \mathbb{C}^{N_{RX}}$ is the received signal for the RE $[n_F, n_S]$ and given as

$$\mathbf{y}_{n_F, n_S} = \mathbf{H}_{n_F, n_S} \mathbf{x}_{n_F, n_S} + \mathbf{w}_{n_F, n_S} \quad (2)$$

where $\mathbf{x}_{n_F, n_S} = [x_{n_F, n_S, 1}, \dots, x_{n_F, n_S, N_{TX}}]^T \in \mathbb{C}^{N_{TX}}$ is the vector of transmitted baseband symbols, $\mathbf{H}_{n_F, n_S} \in \mathbb{C}^{N_{RX} \times N_{TX}}$ is the channel matrix, and $\mathbf{w}_{n_F, n_S} \sim \mathcal{CN}(\mathbf{0}, \sigma^2 \mathbf{I}_{N_{RX}})$ is the complex-valued additive white Gaussian noise (AWGN) with noise power σ^2 . Additional effects such as hardware impairments could be easily integrated in this model.

A. 5G NR PUSCH terminology and structure

We introduce the 5G NR related terminology required to understand the following receiver implementation. For further details, we refer the interested reader to [13].² In 5G NR, each *frame* comprises 10 subframes, each of duration 1 ms. Each one of these subframes is partitioned into *slots*, each consisting of 12 or 14 OFDM symbols. The number of slots depends on the *numerology* defining the subcarrier spacing which takes values ranging from 15 kHz to 120 kHz, e.g., for

²An interactive 5G NR PUSCH tutorial is available online https://nvlabs.github.io/sionna/examples/5G_NR_PUSCH.html.

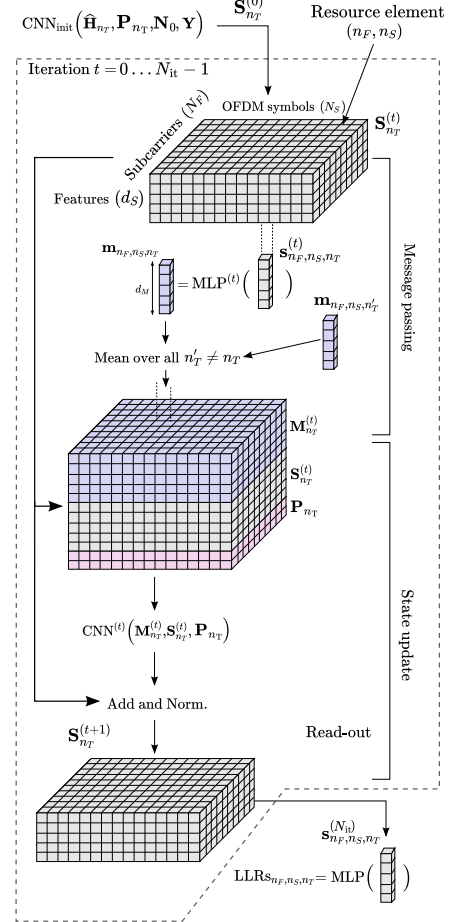


Fig. 2: Architecture of the neural receiver used for MU-MIMO detection. The detection process is shown for layer n_T . Information from other layers n'_T is considered in the message passing step.

30 kHz each frame consists of 20 slots. The subcarriers are grouped into PRBs where each PRB denotes 12 subsequent subcarriers. Further, the so-called DMRS denotes the pilot symbols for channel estimation at pre-defined positions in each slot (see [13, Chapter 9.11]). We configure the system such that the DMRS occurs at OFDM symbol 2 and 11. Each layer is assigned an individual DMRS *port*. It is worth noting that the DMRS positions are fixed within a frame, however, the pilot symbols itself depend on the actual slot number within the frame. The proposed neural receiver operates on a *per-slot* basis, i.e., the received resource grid of 14 consecutive OFDM symbols which represent an entire transport block of 67584 information bits per layer for our configuration.

Algorithm 1: Neural MU-MIMO receiver

Input : Number of iterations N_{it}
Number of layers N_T
Received post-FFT signal $\mathbf{Y} \in \mathbb{C}^{N_F, N_S, N_{RX}}$
Pos. encoded pilot distance $\mathbf{P}_{n_T} \in \mathbb{R}^{N_F, N_S, 2}$
for each layer n_T
[Optional] Noise power spectral density
 $\mathbf{N}_0 \in \mathbb{R}^{N_F, N_S, N_{RX}}$ in dB

Output: Soft-estimate $\ell \in \mathbb{R}^{N_F, N_S, N_T, m}$ for each (coded) bit for each layer

- 1 **For** $n_T = 0, \dots, N_T - 1$
- 2 # Initial LS estimation & interpolation (see (3))
- 3 $\hat{\mathbf{H}}_{n_T} \leftarrow \text{LS_estimate}(\mathbf{Y}, n_T)$
- 4 # Input Embedding (see Fig. 3)
- 5 $\mathbf{S}_{n_T}^{(0)} \leftarrow \text{CNN}_{\text{init}}(\mathbf{Y}, \mathbf{P}_{n_T}, \mathbf{N}_0, \hat{\mathbf{H}}_{n_T})$
- 6 # Run receiver iterations
- 7 **For** $t = 0, \dots, N_{it} - 1$
- 8 **For** $n_T = 0, \dots, N_T - 1$
- 9 # Message passing
- 10 $\mathbf{m}'_{n_F, n_S, n_T} \leftarrow \text{MLP}_{\text{MP}}^{(t)}(\mathbf{s}_{n_F, n_S, n_T}^{(t)}) \quad \forall n_F, n_S$
- 11 # Aggregate states (assuming $N_T \geq 2$)
- 12 $\mathbf{m}_{n_F, n_S, n_T}^{(t)} \leftarrow \frac{1}{N_T - 1} \sum_{n'_T \neq n_T} \mathbf{m}'_{n_F, n_S, n'_T} \quad \forall n_F, n_S$
- 13 # Update states (see Fig. 4)
- 14 $\mathbf{S}_{n_T}^{(t+1)} \leftarrow \text{CNN}_{\text{state}}(\mathbf{M}_{n_T}, \mathbf{P}_{n_T}, \mathbf{S}_{n_T}^{(t)})$
- 15 # Read-out function
- 16 **For** $n_T = 0, \dots, N_T - 1$
- 17 $\ell_{n_F, n_S, n_T} \leftarrow \text{MLP}_{\text{readout}}(\mathbf{S}_{n_F, n_S, n_T}^{(N_{it})}) \quad \forall n_F, n_S$
- 18 **return** ℓ

B. Neural Receiver Architecture

Alg. 1 implements the neural receiver that is shown in Fig. 2. It processes an entire *slot* and provides a one-shot estimation of all transmitted bits of all layers simultaneously. The neural receiver takes as input:³

- The complex-valued received *post-FFT* signal \mathbf{Y} as a 3-dimensional tensor of shape $N_F \times N_S \times N_{RX}$.
- The real-valued positional encoding (PE) \mathbf{P}_{n_T} that provides the normalized distance to the nearest pilot in time (OFDM symbols) and frequency (subcarriers). This is provided as a 3-dimensional tensor of shape $N_F \times N_S \times 2$. As the pilot pattern is specific to each user, \mathbf{P}_{n_T} is also user specific. The implementation is shown in Alg. 2.
- Optionally, the real-valued noise power spectral density \mathbf{N}_0 as a tensor of shape $N_F \times N_S \times N_{RX}$ in dB. Logarithmic scale is used to facilitate operating over large ranges of signal-to-noise ratio (SNR). If not provided the neural receiver can also learn an implicit SNR estimation.
- Optionally, a complex-valued channel estimate $\hat{\mathbf{H}}_{n_T}$ of shape $N_F \times N_S \times N_{RX}$. A least squares (LS) estimate of the channel vector for layer n_T can be obtained for every

³The actual implementation is batched, i.e., multiple slots and layers are processed in parallel. However, for readability this is omitted in the following description.

Algorithm 2: Positional pilot encoding

Input : Set of pilot positions \mathcal{P}_{n_T} for layer n_T
Output: Positional pilot encoding $\mathbf{P}_{n_T} \in \mathbb{R}^{N_F, N_S, 2}$

- 1 **For** $n_F = 1, \dots, N_F$
- 2 **For** $n_S = 1, \dots, N_S$
- 3 # Find closest pilot distance in time
- 4 $\hat{p}_S \leftarrow \min_{\mathbf{p} \in \mathcal{P}_{n_T}} (|p_S - n_S|)$
- 5 # Find closest pilot distance in frequency
- 6 $\hat{p}_F \leftarrow \min_{\mathbf{p} \in \mathcal{P}_{n_T}} (|p_F - n_F|)$
- 7 # Store distance in $\tilde{\mathbf{P}}$
- 8 $\tilde{\mathbf{P}}_{n_F, n_S} \leftarrow [\hat{p}_S, \hat{p}_F]$
- 9 # Normalize to unit variance and zero mean
- $\mathbf{P}_{n_T} \leftarrow \text{norm}(\tilde{\mathbf{P}})$
- 10 **return** \mathbf{P}_{n_T}

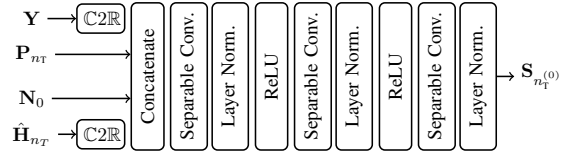


Fig. 3: Architecture of the CNN used to compute the initial state tensor for every user. All separable convolutional layers use kernels of size 3×3 . The first two separable convolutional layers use 128 kernels, and the last one uses d_S units.

RE carrying a pilot according to

$$\hat{\mathbf{h}}_{n_F, n_S, n_T} = \frac{p_{n_F, n_S, n_T}^* \mathbf{y}_{n_F, n_S}}{|p_{n_F, n_S, n_T}|^2} \quad (3)$$

where $p_{n_F, n_S, n_T} \in \mathbb{C}$ is the pilot signal transmitted by layer n_T on the RE $[n_F, n_S]$. Linear interpolation may then be used to obtain estimates of the channel vectors for data-carrying REs. Feeding the receiver with an estimate of the channel coefficients was experimentally found to improve the performance, as it may serve as a bootstrap for channel estimation. This also helps in scenarios where multiple users share the same code division multiplexing (CDM) group and the initial channel estimation can simplify the initial layer separation. Further, the LS estimator introduces only a slight increase in complexity.

The essential processing steps of Alg. 1 consist of three stages: an initialization step, N_{it} unrolled iterations, and a read-out step. During inference, the read-out step is only required in the last iteration. We outline the three stages hereafter:

Initialization step: The initialization step consists of a small CNN, whose architecture is shown in Figure 3. The complex-valued inputs are converted to real-valued tensors by concatenating the real and imaginary components along the feature dimension. Separable convolutions with rectified linear unit (ReLU) activations are used to reduce complexity. The task of this CNN is to compute an initial state tensor of shape $N_F \times N_S \times d_S$ for every layer n_T , denoted by $\mathbf{S}_{n_T}^{(0)}$ and the hyperparameter d_S is the size of the feature dimension. The state tensor of layer n_T holds information about the channel and data for this layer and for every RE $[n_F, n_S]$.

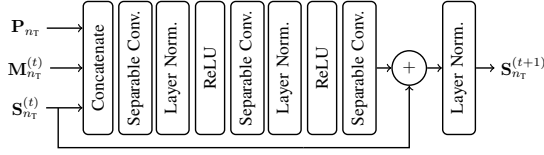


Fig. 4: Architecture of the CNN used to update the state of every layer. All separable convolutional layers use kernels of size 3×3 . The first two separable convolutional layers use 256 kernels, and the last one uses d_S kernels.

Unrolled iterative algorithm: The main stage of the proposed neural receiver consists of an unrolled iterative algorithm with N_{it} iterations. Each iteration updates the state tensor of every layer from $\mathbf{S}_{n_T}^{(t)}$ to $\mathbf{S}_{n_T}^{(t+1)}$, $0 \leq t \leq N_{it} - 1$. Each iteration consists of the following two steps.

a) *Message passing:* The first step consists of message passing between all layers performed individually for every RE $[n_F, n_S]$. Given an RE $[n_F, n_S]$, the state of each layer n_T is computed using a multilayer perceptron (MLP) according to

$$\mathbf{m}'_{n_F, n_S, n_T} = \text{MLP}^{(t)} \left(\mathbf{s}_{n_F, n_S, n_T}^{(t)} \right) \quad (4)$$

where $\mathbf{s}_{n_F, n_S, n_T}^{(t)} \in \mathbb{R}^{d_S}$ is the sub-vector of $\mathbf{S}_{n_T}^{(t)}$ corresponding to the RE $[n_F, n_S]$ and $\mathbf{m}' \in \mathbb{R}^{d_M}$. One may consider $\mathbf{s}_{n_F, n_S, n_T}^{(t)}$ as carrying the data and channel information for the RE $[n_F, n_S]$ of layer n_T , where the hyperparameter d_M is the size of the messages. The MLP has a single hidden layer with ReLU activations. Note that the same MLP is used for all pairs of layers and for all REs.

The messages intended for layer n_T are then aggregated as

$$\mathbf{m}_{n_F, n_S, n_T} = \begin{cases} \frac{1}{N_T - 1} \sum_{n'_T \neq n_T} \mathbf{m}'_{n_F, n_S, n'_T} & \text{if } N_T \geq 2 \\ \mathbf{0} & \text{if } N_T = 1 \end{cases} \quad (5)$$

to form the message tensor $\mathbf{M}_{n_T}^{(t)}$ of shape $N_F \times N_S \times d_M$.

b) *State update:* The second step of every iteration consists in updating the state tensor of every layer n_T from the message tensor $\mathbf{M}_{n_T}^{(t)}$, the current state tensor $\mathbf{S}_{n_T}^{(t)}$, and the PE \mathbf{P}_{n_T} . This is implemented independently for all layers, using a CNN whose architecture is shown in Fig. 4. A skip connection is used to avoid vanishing gradients, and separable convolutions with ReLU activations to reduce complexity. The same CNN is used for all layers. Using a CNN enables exploiting the time-frequency correlation of the channel coefficients, while taking into account the interference from the other users through the message tensor. Weight sharing across iterations was found to significantly degrade the performance and hence cannot be used.

Read-out: The last stage consists of computing log-likelihood ratios (LLRs) $\ell_{n_F, n_S, n_T}^{(t)} \in \mathbb{R}^m$ for the m bits $\mathbf{b}_{n_F, n_S, n_T}$ transmitted by the layer over this RE for every layer n_T and every RE $[n_F, n_S]$. This is achieved using a read-out network implemented by an MLP, that individually processes the state vectors $\mathbf{s}_{n_F, n_S, n_T}^{(t)}$ of every RE and layer, such that

$$\ell_{n_F, n_S, n_T}^{(t)} = \text{MLP}_{\text{readout}}(\mathbf{S}_{n_F, n_S, n_T}^{(t)}) \quad \forall n_F, n_S, n_T.$$

Algorithm 3: Training Loop

Input : Batch size B , learning rate l
Number training iterations $N_{\text{train, it}}$
SNR range $[\sigma_{\min}^2, \sigma_{\max}^2]$
Max. number of layer $N_{T, \max}$
Initial weights $\theta^{(0)}$

Output: Optimized weights θ^*

```

1 # Apply  $N_{\text{train, it}}$  SGD training iterations
2 For  $t = 0, \dots, N_{\text{train, it}} - 1$ 
3   # Sample random number of layers
4    $N_T \leftarrow \text{triangleSampler}(1, N_{T, \max})$ 
5    $\mathcal{L} \leftarrow 0$  # Average loss over batch
6   For  $0, \dots, B$ 
7     # Sample random SNR
8      $\sigma^2 \leftarrow \text{SNRSampler}(\sigma_{\min}^2, \sigma_{\max}^2)$ 
9     # Draw new random channel realization
10     $\mathbf{H} \leftarrow \text{getChannel}(N_T)$ 
11    # Sample random bits  $\mathbf{B}$  and simulate
12    # transmission
13     $\mathbf{Y}, \mathbf{B} \leftarrow \text{simTransmission}(\mathbf{H}, \sigma^2, N_T)$ 
14    # Apply neural receiver
15     $\ell \leftarrow \text{runNeuralRX}(\mathbf{Y}, \theta^{(t)}, N_T)$ 
16    # Calculate and accumulate BCE loss from (6)
17     $\mathcal{L} \leftarrow \mathcal{L} + \text{calcLoss}(\ell, \mathbf{B})$ 
18    # Apply SGD and update weights
19     $\theta^{(t+1)} \leftarrow \text{SGD}(\mathcal{L}/B, \theta^{(t)}, l)$ 
20 return  $\theta^* \leftarrow \theta^{N_{\text{train, it}}}$ 

```

Note that the same MLPs are used for all layers and for all REs. As a result, the entire network consists of approximately 730k trainable weights.

C. Training & Generalization

The proposed neural receiver architecture is fully differentiable and, hence, stochastic gradient descent (SGD)-based training is straightforward. We use the adaptive momentum (ADAM) optimizer with learning rate $l = 10^{-3}$, and the binary cross-entropy (BCE) loss function. Thus, the neural receiver can be seen as attempting to solve $N_F \times N_S \times N_T \times m$ binary classification problems⁴ in parallel from the received signal \mathbf{Y} . The detailed training algorithm can be found in Alg. 3. We can estimate the BCE by Monte-Carlo integration

$$\begin{aligned} \mathcal{L} \approx & -\frac{1}{BN_F N_S N_T m} \sum_{b=0}^{B-1} \sum_{n_F=1}^{N_F} \sum_{n_S=1}^{N_S} \sum_{n_T=0}^{N_T-1} \sum_{i=0}^{m-1} \\ & \left[b_{n_F, n_S, n_T, i}^{[b]} \log_2 \left(\sigma \left(\ell_{n_F, n_S, n_T, i} \left(\mathbf{Y}^{[b]} \right) \right) \right) \right. \\ & \left. + \left(1 - b_{n_F, n_S, n_T, i}^{[b]} \right) \log_2 \left(\sigma \left(-\ell_{n_F, n_S, n_T, i} \left(\mathbf{Y}^{[b]} \right) \right) \right) \right] \quad (6) \end{aligned}$$

where B is the batch size, the superscript $[b]$ is used to refer to the b^{th} batch example, and $\sigma(\cdot)$ is the logistic sigmoid

⁴For readability, we ignore the fact that some REs are allocated to pilots in the following description, however, in the actual implementation these positions are excluded from the calculation of the loss.

function. $\ell_{n_F, n_S, n_T, i}(\mathbf{Y})$ denotes the LLR computed by the detector from the received signal \mathbf{Y} for the i^{th} bit of layer n_T transmitted over the RE $[n_F, n_S]$. As LLRs are binary logits, $\sigma(\ell_{n_F, n_S, n_T, i}(\mathbf{Y}))$ gives the corresponding probability for the bit to be equal to one given \mathbf{Y} . For training, we average the loss over all iterations to ensure that inference of the receiver can be done for a flexible number of iterations (see *multi-loss* in [14]). Moreover, training on the BCE was shown to be equivalent to minimizing the Kullback–Leibler (KL) divergence between the posterior distribution on the bits approximated by the neural receiver and the true one that would be given by an optimal receiver (cf. [15]). Further, the LLRs after channel decoding can be used for training if the channel decoder is differentiable (e.g., for belief propagation (BP) decoding [14]). However, we empirically did not observe any gains by doing so.

To account for a flexible number of layers, we randomly sample a different number of active users for every batch, i.e., per SGD iteration. Intuitively, the task of MU-MIMO detection becomes more complicated if a larger number of users is active and, therefore, we use a triangular distribution for the number of active layers [8] such that scenarios with many active layers occur more frequently.

To avoid overfitting to a particular channel condition, the neural receiver was trained on the 3GPP UMi model built in Sionna [12], with a random drop of users for every batch example. This ensures that the NN does not overfit to specific power delay profiles and angles of arrival and departure. Moreover, the user speeds are independently and uniformly sampled from the range $[0, 34] \text{ ms}^{-1}$ at training. This procedure ensures that the resulting neural receiver generalizes well to unseen channel realizations. For training with real world data, one can also embed actual measurements in the synthetic training dataset to ensure that the receiver still generalizes as the acquisition of samples from many different channel measurements turns out to be cumbersome and expensive.

III. RESULTS EVALUATION

For our experiments, we use the Sionna [12] link-level simulator to train and evaluate the neural receiver. For all experiments, we focus on the 5G NR PUSCH scenario and set $N_S = 14$ OFDM symbols per slot (see Sec. II-A for details). For the training, the number of PRBs is set to 4 (i.e., $N_F = 48$ sub-carriers) and 217 PRBs (i.e., $N_F = 2604$ sub-carriers) for the evaluation, respectively. This underlines that the neural receiver shall support a variable number of subcarriers. The carrier frequency is set to 2.14 GHz and the subcarrier spacing is 30 kHz. We use the 3GPP UMi model [16] with randomized user positions and user speeds between 0 ms^{-1} and 34 ms^{-1} . Further, the modulation and coding scheme (MCS) index is set to 14, leading to Gray labelled 16-QAM, and low-density parity-check (LDPC) code of rate 0.54 throughout all experiments. Note that the code rate can be changed without the need for retraining, however, the QAM constellation is *baked* into the weights of the model. The same

holds for the sub-carrier spacing, so that changing from 30 kHz to 60 kHz requires retraining of the current network.

A. Varying number of layers

One of the key challenges of neural networks is the possibility to re-parametrize the network without the need for retraining. The number of receive antennas is set to $N_{\text{RX}} = 16$, and the neural receiver is trained with a randomly sampled number of active layers, N_T , ranging from 1 to 4. Note that in our configuration, there are only two CDM groups and two users must share the same CDM group, i.e., their pilots are transmitted on the same resource elements.

The results in Fig. 5 show the transport block error rate (TBLER) evaluation for the *same* neural receiver for a different number of active users without any additional retraining. We compare the neural receiver to a conventional baseline using LS channel estimation at pilot locations and linear interpolation across the data symbols, and linear minimum mean square error (LMMSE) equalization. Further, we show a baseline using LMMSE channel estimation with K-best detection which has a high computational complexity, but can be considered as an approximation of maximum likelihood detection. As one can see, the proposed architecture outperforms the LS baseline in all scenarios and operates at a performance close to the baseline using LMMSE channel estimation with K-best detection, but at a significantly lower computational complexity. Further, the error floor is significantly lower with the neural receiver, suggesting that it implicitly performs a more accurate channel estimation than the two other schemes.

B. Hardware-in-the-loop & 3GPP conformance test

As a final experiment, we validate our implementation with 5G NR MU-MIMO RF signals in a hardware-in-the-loop setup based on the R&S@SMW200A vector signal generator, the R&S@MSR4 multi-purpose (satellite) receiver, and a signal analysis software framework to pre-process the received signals (synchronization, FFT calculation). With this setup, we emulate two users ($N_T = 2$), each equipped with two transmit antennas, and use the four inputs of the receiver with $N_{\text{RX}} = 4$ antennas. We use 217 PRBs for the hardware setup. To account for the different channels of both users at different positions, we emulate two different tapped delay line (TDL) models from the 3GPP 38.901 conformance test cases in the signal generator:

- TDL-B100/400: TDL-B with 100ns delay spread and 400Hz Doppler shift [16]
- TDL-C300/100: TDL-C with 300ns delay spread and 100Hz Doppler shift [16]

The receiver *sees* the superposition of the two channel outputs with an additional AWGN component. We want to emphasize that the receiver is *not* trained for this specific channel model and, thus, can operate on any random realization of the entire *ensemble* of possible UMi channels.

Fig. 6 shows the block error rate (BLER) at transport block level including all physical layer effects of an entire slot. As can be seen, the neural receiver operates close to

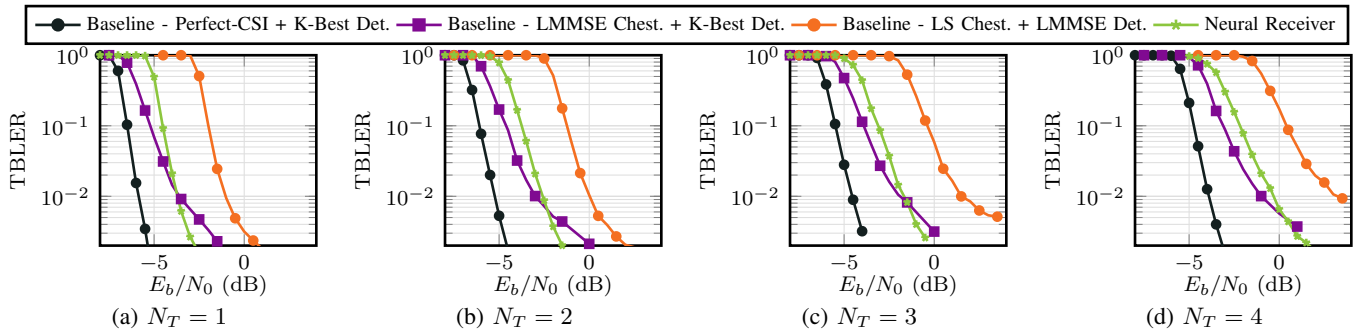


Fig. 5: Varying number of active layers N_T for a 3GPP UMi channel model and $N_{RX} = 16$ receive antennas. The receiver was trained for $N_{T,max} = 4$. We randomize for every sample the user positions and user mobility from 0 to 34 m s^{-1} .

the baseline consisting of LMMSE channel estimation with K-best detection but at a significantly lower computational complexity. Further, the neural receiver outperforms the more practical receiver using LS channel estimation and LMMSE-based detection significantly. While the solid green curve is a simulated result, the blue dots indicate the measured TBLE for the actual experiment. The small performance mismatch can be explained by the aggregation of all hardware effects (quantization noise, carrier frequency offset, ...) which are not considered in the simulations. Further, slightly different numerical implementations of the channel models are possible.

IV. CONCLUSION

We have presented a neural MU-MIMO OFDM receiver and demonstrated its 5G NR PUSCH compatibility. The proposed receiver outperforms our classical baselines and is flexible with respect to the number of layers and PRBs. Beyond pure block error-rate performance gains, our plan is that these receivers can be finetuned for a specific environment considering the site-specific properties such as the expected user speed (e.g., highway vs. indoor scenarios) or the expected maximum delay spread for the area of interest. As such, we envision base stations that are continuously retrained—during low-load phases—and, thereby, improve their performance even after deployment in the field by simple weight updates.

Going further, neural receivers can be seen as an enabler for a plethora of new physical layer concepts such as AI/ML-based waveforms [2], [4] or even semantic communications. We leave it open for future work to optimize the architecture towards real-time inference. The flexibility w.r.t. the modulation schemes is an interesting and important challenge. A possible approach for such a flexibility could be in input embeddings that account for the actual modulation scheme.

REFERENCES

- [1] M. Honkala, D. Korpi, and J. M. Huttunen, "DeepRX: Fully Convolutional Deep Learning Receiver," *IEEE Trans. Wirel. Commun.*, vol. 20, no. 6, pp. 3925–3940, 2021.
- [2] T. O’Shea and J. Hoydis, "An Introduction to Deep Learning for the Physical Layer," *IEEE Trans. on Cognitive Commun. and Netw.*, vol. 3, no. 4, pp. 563–575, 2017.
- [3] X. Lin, "Artificial Intelligence in 3GPP 5G-Advanced: A Survey," *arXiv preprint arXiv:2305.05092*, 2023.
- [4] F. Ait Aoudia and J. Hoydis, "End-to-end learning for OFDM: From Neural Receivers to Pilotless Communication," *IEEE Transactions on Wireless Communications*, vol. 21, no. 2, pp. 1049–1063, 2021.

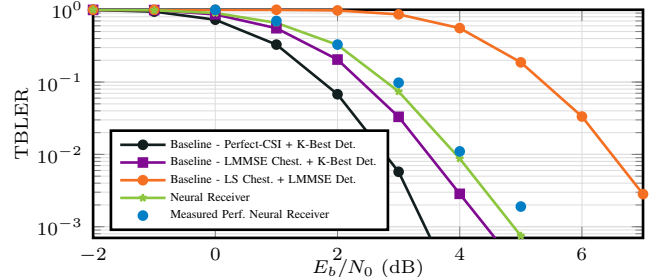


Fig. 6: Hardware-in-the-loop results for $N_T = 2$ user MIMO with $N_{RX} = 4$ receiver antennas and TDL-B100/400 & TDL-C300/100 channels. No retraining for the TDL channel is done.

- [5] H. Ye, G. Y. Li, and B.-H. Juang, "Power of Deep Learning for Channel Estimation and Signal Detection in OFDM Systems," *IEEE Wireless Communications Letters*, vol. 7, no. 1, pp. 114–117, 2017.
- [6] D. Korpi, M. Honkala, J. M. Huttunen, and V. Starck, "DeepRX MIMO: Convolutional MIMO Detection with Learned Multiplicative Transformations," in *ICC 2021-IEEE International Conference on Communications*. IEEE, 2021, pp. 1–7.
- [7] N. Soltani, H. Cheng, M. Belgiovine, Y. Li, H. Li, B. Azari, S. D’Oro, T. Imbirba, T. Melodia, P. Closas *et al.*, "Neural Network-based OFDM Receiver for Resource Constrained IoT Devices," *IEEE Internet of Things Magazine*, vol. 5, no. 3, pp. 158–164, 2022.
- [8] K. Pratik, B. D. Rao, and M. Welling, "RE-MIMO: Recurrent and Permutation Equivariant Neural MIMO Detection," *IEEE Transactions on Signal Processing*, vol. 69, pp. 459–473, 2021.
- [9] M. Khani, M. Alizadeh, J. Hoydis, and P. Fleming, "Adaptive Neural Signal Detection for Massive MIMO," *IEEE Transactions on Wireless Communications*, vol. 19, no. 8, pp. 5635–5648, 2020.
- [10] A. Scotti, N. N. Moghadam, D. Liu, K. Gafvert, and J. Huang, "Graph Neural Networks for Massive MIMO Detection," *arXiv preprint arXiv:2007.05703*, 2020.
- [11] A. Kosasih, V. Onasis, W. Hardjawana, V. Miloslavskaya, V. Andrean, J.-S. Leu, and B. Vucetic, "Graph Neural Network Aided Expectation Propagation Detector for MU-MIMO Systems," in *IEEE Wireless Communications and Networking Conference*, 2022, pp. 1212–1217.
- [12] J. Hoydis, S. Cammerer, F. Ait Aoudia, A. Vem, N. Binder, G. Marcus, and A. Keller, "Sionna: An Open-Source Library for Next-Generation Physical Layer Research," *preprint arXiv:2203.11854*, 2022.
- [13] E. Dahlman, S. Parkvall, and J. Skold, *5G NR: The Next Generation Wireless Access Technology*. Academic Press, 2020.
- [14] E. Nachmani, Y. Be’ery, and D. Burshtein, "Learning to Decode Linear Codes Using Deep Learning," in *IEEE Annual Allerton Conference on Communication, Control, and Computing*, 2016, pp. 341–346.
- [15] M. Stark, F. Ait Aoudia, and J. Hoydis, "Joint Learning of Geometric and Probabilistic Constellation Shaping," in *2019 IEEE Globecom Workshops*. IEEE, 2019, pp. 1–6.
- [16] ETSI, "3GPP TR 38.901, "Study on channel model for frequencies from 0.5 to 100 GHz", Release 16.1," Tech. Rep.